Microfluidic Assisted Nanoprecipitation of PLGA Nanoparticles for Curcumin Delivery to Leukemia Jurkat Cells

Mandy H. M. Leung and Amy Q. Shen*

Micro/Bio/Nanofluidics Unit, Okinawa Institute of Science and Technology Graduate University, 1919-1 Tancha, Onna-son, Kunigami-gun, Okinawa, 904-0495 Japan

E-mail: amy.shen@oist.jp

Phone: +81-(0)98-982-3374. Fax: +81-98-982-3420

Abstract

The ability to control particle size and size distribution of nanoparticles for drug delivery is essential because it impacts on the biodistribution and cellular uptake of nanoparticles. We present a novel microfluidic assisted nanoprecipitation strategy that enables synthesis of surfactant-free curcumin encapsulated poly(lactide-co-glycolide) nanoparticles (Cur-PLGA NP) with adjustable particle diameters (30–70 nm) and narrow particle size distribution (polydispersity index less than 0.2). Our Cur-PLGA NP exhibit excellent colloidal stability and inhibit degradation of curcumin. We further demonstrate the potential of our Cur-PLGA NP as a nanotoxic delivery system for curcumin. Cellular viability assay validates a dose-dependent cytotoxicity of Cur-PLGA NP in leukemia Jurkat cells. In contrast, Cur-PLGA NP does not alter the viability of fibroblast NIH3T3 cells, which suggests that the cytotoxicity of Cur-PLGA NP is specific to cell types. Furthermore, there is no detectable effect by PLGA NP to both leukemia Jurkat cells and fibroblast NIH3T3 cells, highlighting the nontoxic nature of

our delivery system. Confocal cell uptake studies indicate that PLGA NP do not alter the cell uptake of curcumin. Our microfluidic assisted approach offers a controlled and effective nano-biomaterials synthesis of drug delivery system for curcumin, which can be extended to different capsule materials for a variety of biomedical applications.

INTRODUCTION

Amongst all the FDA-approved biodegradable polymers, poly(lactide-*co*-glycolide) (PLGA, Figure 1a) has demonstrated immense potential as a drug delivery carrier due to its excellent biocompatibility and biodegradability.[1–3] It has been shown that PLGA nanoparticles (PLGA NP) are biocompatible, which are hydrolyzed into smaller units and further degraded by cells.[4,5] It has been validated that PLGA NP is useful in encapsulating curcumin to enhance its aqueous solubility and stability.[1–3,6–8] Curcumin (Figure 1a), the yellow pigment found in turmeric, exhibits various medicinal properties, including anti-cancer, anti-Alzheimer's and anti-inflammatory activities.[1–3,9–12] However, the poor aqueous solubility and the instability of curcumin hinder its bioavailability. Curcumin has a solubility of only $10\,\mu g\,mL^{-1}$ in water due to its hydrophobicity but its solubility increases in polar organic solvents.[13,14] Also, the hydrolysis of curcumin has been linked to its degradation mechanism with 50 % of curcumin degraded within 30 min in a pH 7.4 phosphate buffer solution.[15,16] Recently, PLGA NP have been employed to deliver curcumin efficiently into cancer cells,[1–3] with curcumin effectively inhibiting cancer cell proliferation.[2] This anti-proliferation effect has been linked to alteration of the cell cycle by curcumin, which reduces the S phase and blocks the G2/M phase.[2] In addition, curcumin-PLGA nanoformulation induces apoptosis by inhibiting NFκB activation.[2,17] Therefore, PLGA NP are effective delivery agents for curcumin and they do not alter curcumin's medicinal effect.

A previous study has shown that curcumin encapsulated PLGA NP (Cur-PLGA NP) can be synthesized using a stabilizer-free one-step nanoprecipitation method.[6] The stabilizer-free nanoprecipitation provides a simple system for direct study of the PLGA NP without any

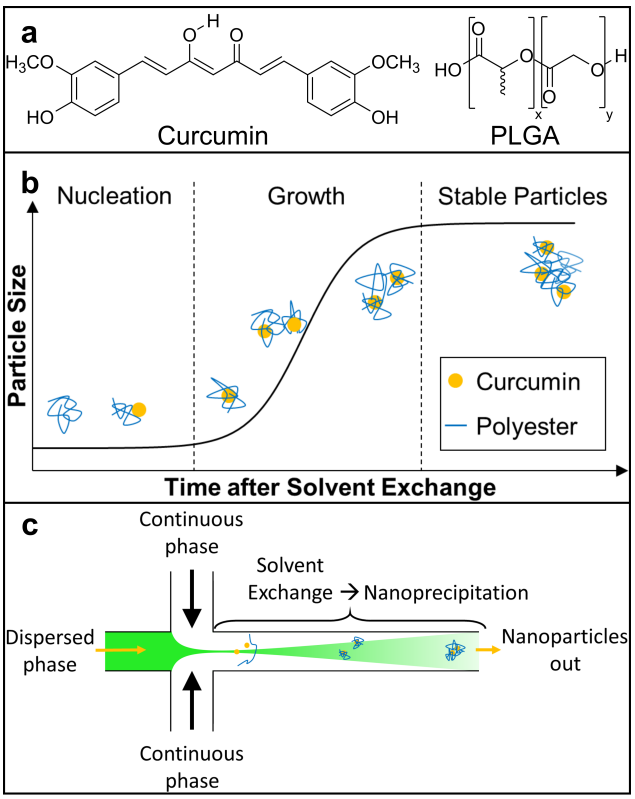

Figure 1: (a) Chemical structure of curcumin and poly(D,L-lactide-*co*-glycolide) (PLGA). (b) Mechanism of Cur-PLGA NP nanoprecipitation by solvent exchange. (c) Schematic of nanoprecipitation by hydrodynamic flow focusing in a cross slot microfluidic device.

biases in nanoparticle sizing and eliminates any additional effects may have on cells by the stabilizers.[6,18,19] Stable Cur-PLGA NP of approximately 100 nm in diameter were formed by nanoprecipitation because the solubility of curcumin and PLGA decreases upon exchange of acetone by water.[6] Nanoprecipitation via solvent exchange requires two miscible solvents, with both PLGA and curcumin being dissolved in one system (the solvent), but not in the other (the non-solvent). Nanoprecipitation involves three stages: nucleation, growth and formation of stable particles as illustrated in Figure 1b.[20] First, nucleation occurs when the solution has passed supersaturation due to rapid diffusion of the solvent into the non-solvent phase. Second, particle growth occurs upon collision, which is governed by diffusion of curcumin and PLGA molecules. Finally, an equilibrium is reached as particles are kinetically stable when the energy barrier for aggregation is too high. Homogeneous supersaturation, which requires that the mixing of the solvent and the non-solvent phases, is very critical

for formation of small particles because rapid mixing results in a high nucleation rates and formation of smaller nuclei.[20] In another word, the mixing time of the solvent and the non-solvent phases must be less than the time scale for nanoparticle aggregation in order to achieve small particles.[21]

It is well established that nanoparticles accumulate in tumors due to enhanced permeability and retention (EPR) of defective vessels and inefficient lymphatic drainage, one of the underlying mechanisms to deliver drugs encapsulated in nanoparticles.[22,23] Particle size is critical for EPR effect as particles with size less than 10 nm are easily cleared by the kidneys and the pore cut-off size of blood vessels is about 100 nm.[22,23] Therefore, particles between 10 nm and 100 nm can be passively accumulated in tumors by EPR. It has been suggested that the slow and uncontrolled mixing of solvent in a typical nanoprecipitation synthesis is responsible for the formation of larger nanoparticles with a wide particle size distribution.[20,21] Previous stabilizer-free one-step nanoprecipitation method gives Cur-PLGA NP of approximately 100 nm in diameter with a particle size distribution across 20 to 120 nm.[6] In response to this challenge, microfluidic reactor has emerged as a powerful platform to provide rapid and controlled mixing of solutions, which decreases the mixing time, leading to formation of smaller nanoparticles with a narrower size distribution compared to those from traditional nanoprecipitation methods.[21,24–26]

The primary aim of this work is to synthesize surfactant-free Cur-PLGA NP with particle diameters less than 100 nm and a narrow size distribution to achieve the EPR effect, by using controlled nanoprecipitation with a microfluidic platform. Figure 1c illustrates the nanoprecipitation of Cur-PLGA NP using hydrodynamic flow focusing inside a cross slot microfluidic device. The microfluidic synthesized PLGA NP not only exhibit a suppression of curcumin degradation, but also act as an efficient delivery agent for curcumin. The anti-cancer effect of the synthesized Cur-PLGA NP is also evaluated by using luekemia Jurkat cells and NIH3T3 fibroblast cells for *in vitro* studies. The *in vitro* cell studies demonstrate that the microfluidic synthesized PLGA NP has great potential as a drug delivery system

for curcumin.

EXPERIMENTAL SECTION

Materials

Curcumin (purity >98%) and poly(D,L-lactide-*co*-glycolide) (PLGA, acid terminated, 50:50 lactide:glycolide, M_w: 24 000 to 38 000) were purchased from Sigma Aldrich (Japan). Acetone and triethylamine from Nacalai (Japan) and ethyl acetate from Wako (Japan) were used as received. Water from a Millipore Milli-Q NANOpure water system was used in all experiments. Leukemia Bcl-2 (S70A) Jurkat and NIH3T3 (mouse embryonic fibroblast) cell lines are from ATCC (USA). RPMI 1640 media and Dulbecco's modified Eagle medium (DMEM) were purchased from Invitrogen (USA). Jurkat cells were grown in RPMI 1640 media containing 10 % fetal bovine serum. NIH3T3 cells were grown in DMEM containing 10 % iron fortified calf serum. All media contain 1 % geneticin. Cells were cultured at 37 °C in a humidified atmosphere of 5 % CO_2.

Microfluidic device fabrication

The microfluidic devices were fabricated using soft lithography.[27] In brief, the cross slot microfluidic device (Figure 1c) with channel width of 20 µm were designed with AutoCAD (AutoDesk, USA). A layer of DWL 40 photoresist with a thickness of 60 µm was coated onto a 4-inch in diameter silicon wafer. The features of the cross slot microfluidic device were patterned by photolithgraphy using a DL1000 maskless writer (NanoSystem Solutions, Japan) and developed by using a mr-Dev 600 developer (Microresist Technologies, Germany). The wafer was subsequently coated with an anti-adhesive layer by exposing it to trichloro(1*H*,1*H*,2*H*,2*H*-perfluorooctyl)silane (Sigma Aldrich, Japan) in the vapor phase in a desiccator for at least 1 h. A mixture of 10:1 poly-(dimethylsiloxane) (PDMS) (Sylgard 184, Dow Corning, Japan) was poured onto the wafer, desiccated and cured for 24 h at 60 °C.

The resulting PDMS cast was peeled off from the wafer, and extracted in the order of triethylamine, ethyl acetate and acetone for 2 h, respectively, to remove the uncross-linked low molecular weight oligomers.[28] The extracted PDMS piece was then dried in a 60 °C oven overnight, followed by air plasma (80 s) bonded onto a glass-slide using a plasma cleaner (Harrick Plasma, USA). The assembled device was then heated at 80 °C for 2 h on a hot plate to strengthen the bonding of the PDMS slab to the glass substrate. The microfluidic device contains one outlet and one inlet for each continuous and dispersed phase, while the inlet for the continuous phase was split into two streams at the flow focusing junction.

Cur-PLGA NP synthesis

A stock solution of curcumin and PLGA in acetone was introduced into the device as dispersed phase through the inserted PTFE tubing (OD: 1/16" and ID: 1/32", OMNIFIT tubing). Syringe pumps (YSP-101 from YMC, Japan) mounted with gas-tight glass syringes were used to control the flow rate of the continuous (SGE Analytical Science, Australia) and dispersed phases (Hamilton, USA). The acetone was then removed under reduced pressure at 40 °C until the volume of the collected Cur-PLGA NP solution was reduced approximately by half to ensure complete removal of acetone. The resulting Cur-PLGA NP solution was kept refrigerated and filtered with a 200 nm syringe-driven filter (Millex from Merck, Germany) to ensure that there is no large aggregates in the sample before testing. The resulting Cur-PLGA solution was kept in the dark environment to limit the exposure to ambient light. The *in situ* nanoprecipitation at the cross slot was imaged using spinning disk and structured illumination hybrid fluorescent confocal imaging (Andor DSD2, Japan) at 20x magnification on an inverted microscope (Ti-E, Nikon, Japan)

Cur-PLGA NP characterization

Images of the synthesized bare PLGA NP and Cur-PLGA NP were taken with Dimension ICON3 atomic force microscope (AFM) with a NanoScope V controller (Bruker, USA).

Nanoparticle suspension was drop-casted onto an atomically flat mica substrate and dried under vacuum. Measurements were performed using silicon cantilevers with a resonance frequency around 300 kHz and a typical tip radius of 7 nm (OTESPA-R3, Bruker, USA) in tapping mode at a scan rate of 1 kHz with a spatial resolution of 256 × 256 pixel. AFM images were processed with NanoScope Analysis (Bruker, USA) and the particle size profile was analyzed by ImageJ for randomly selected 100 particles.[29]

Transmission electron microscopy (TEM) was used to investigate the morphology of bare PLGA NP and Cur-PLGA NP. Nanoparticle suspension was drop-casted onto air plasma activated copper grid (400 mesh) coated with carbon film and dried at ambient temperature after removal of excess solution. To enhance contrast for imaging purposes, the sample was then stained with 1 % (w/v) uranyl acetate (UA) solution before imaging at high vacuum with TEM (JEM-1230R, JEOL, Japan) at 300 kV.

The size distribution of synthesized nanoparticles were characterized by dynamic light scattering (DLS). DLS experiments were performed with a 3D LS spectrometer (LS Instruments, Switzerland) equipped with a HeNe laser operating at 633 nm. The measurements were made at scattering angles ranging from 90° to 135°. Samples were placed in borosilicate cylindrical glass cuvettes (LS Instruments, Switzerland) and allowed 15-min equilibration time at 37 °C prior to data acquisition. The mean hydrodynamic radius and polydispersity index (PDI) of the nanoparticles were determined by the cumulant method.[30] Particle size distributions were determined using CONTIN analysis on the average of 10 measurements.[31]

Zeta potentials of the synthesized nanoparticle were measured using an electrophoretic light scattering spectrophotometer (ELZS-2000, Otsuka Electronics Co., Ltd, Japan). Measurements were taken using a disposable cell with gold-plated electrodes (Otsuka Electronics Co., Ltd, Japan) at 37 °C with a 2-min equilibration time. Zeta potential was calculated from the electrophoretic mobility using the Helmholtz-Smoluchowski equation based on the electrophretic light scattering. Zeta potential values were reported as the mean of three independent measurements and errors were estimated from the standard deviation.

The encapsulation efficiency of the Cur-PLGA NP was determined by dissolving an aliquot of a concentrated Cur-PLGA NP solution in acetone with a final volume of water less than 5 % to extract the encapsulated curcumin. The amount of curcumin presented in Cur-PLGA NP is calculated from the absorbance of curcumin ($A_{420\,nm}$) of the acetone solution measured with a UV-1800 UV-VIS spectrophotometer (Shimadzu, Japan). The amount of curcumin present was calculated from a standard curve of absorbance at 422 nm against the concentration of curcumin in the presence of PLGA in acetone with 1% of water (Supporting Information Figure S.2). The curcumin encapsulation efficiency of PLGA NP is given by:

$$\text{Encapsulation efficiency}\,(\%) = \frac{\text{Amount of curcumin in PLGA NP}}{\text{Amount of curcumin used in the synthesis}} \times 100. \qquad (1)$$

Stability of PLGA NP encapsulated curcumin

Kinetic UV-visible absorption spectra (300 to 800 nm) of the Cur-PLGA NPs were recorded with a UV-1800 UV-VIS spectrophotometer (Shimadzu, Japan). To demonstrate the aqueous stability of the curcumin in PLGA NPs, UV-visible spectra of Cur-PLGA NP solution containing approximately 15 µM of curcumin ($A_{420\,nm} \approx 1$) were collected at 15-min intervals for 12 h, 24 h and 48 h at 37 °C. The concentration of curcumin in the Cur-PLGA NP solution was determined using UV-visible spectroscopy and adjusted with addition of Milli-Q water. To demonstrate the rapid degradation of native curcumin in water, UV-visible spectra of curcumin in water were collected at 15-min intervals for 6 h at 37 °C. To prepare curcumin in an aqueous solution, an aliquot of 2 mg mL^{-1} curcumin in acetone stock was added to Milli-Q water to yield a solution with $A_{420\,nm} \approx 1$. All UV-visible experiments were done in triplicates and results were reported as the mean with the standard deviation of the mean as error.

Fluorescence spectroscopy of Cur-PLGA NP

Fluorescence emission spectrum of the Cur-PLGA NP (430 to 650 nm) was recorded with a Fluorescence Spectrometer F-7000 (Hitachi, Japan). The absorbance of Cur-PLGA NP at 420 nm was adjusted to 0.1 for the fluorescence measurement to minimize the inner filter effect. The excitation used was 420 nm with a 5 nm slit width, while the emission slit width was set at 2.5 nm. The reported fluorescence emission spectrum was the average of three measurements.

Cur-PLGA NP cellular uptake

The qualitative cellular uptake studies involved imaging leukemia Jurkat and NIH3T3 fibroblast cell lines with both the native curcumin and the Cur-PLGA NP treatments. Experiments were repeated three times to ensure the reproducibility. The synthesized Cur-PLGA NP and blank PLGA NP solutions were further concentrated to minimize the hypotonic stress to cells. The concentration of curcumin in the Cur-PLGA NP solution was determined using UV-visible spectroscopy and adjusted with addition of Milli-Q water. The final dosage volume is less than 10 % of the total volume. Cells were washed with 0.5 mL of PBS three times so that only intracellular curcumin was detected before fixation using 4 % paraformaldehyde and staining of cell nucleus with Hoechst 33258 solution (Sigma Aldrich, Japan). The fluorescence images were captured by a Nikon Eclipse Ti-E Spinning Disk (Andor, Japan) confocal microscope and controlled with Andor iQ3 Live Cell Imaging software using the GFP and DAPI channels. The fluorescence intensity of curcumin in cells were measured with a flow cytometer (Accuri C6, Becton Dickinson Biosciences, USA). The blue fluorescence from Hoechst 33258 and the green fluorescence from curcumin were analyzed using the 533/30 and 585/40 filter, respectively. The flow cytometery data were analyzed with FlowJo 10.4.2 (FlowJo LLC, USA).

Cell viability

Cells were seeded at 1×10^4 cells/well in 24-well plates (Thermo Scientific, USA) with various concentrations of Cur-PLGA NP and then incubated for 1 to 3 days. Experiments were repeated three times to ensure the reproducibility. The synthesized Cur-PLGA NP and blank PLGA NP solutions were further concentrated and the concentration of curcumin was determined using UV-visible spectroscopy and adjusted with addition of Milli-Q water. The final dosage volume was less than 10 % of the total volume and the additional water did not induce cell death. To assess the cell viability, cells were stained using the Muse™ Count and Viability Assay Kit and analyzed using a Muse™ Cell Analyzer according to manufacturer's instructions (EMD Millipore, Japan). Both viable and non-viable cells were differentially stained based on their permeability to two DNA-binding dyes in the reagent solution. The cell viability calculations were performed automatically using the Muse™ Count and Viability Software Module. The Cur-PLGA NP dose-response of Jurkat cells was investigated with various concentrations of curcumin in the Cur-PLGA NP solution and analyzed with OriginPro 2016 software (OriginLab, USA).

RESULTS AND DISCUSSION

Microfluidic synthesis of Cur-PLGA NP

A cross slot microfluidic device was fabricated with PDMS bonded to glass for the nano-precipitation by hydrodynamic flow focusing as described in the Introduction. The cured PDMS was extracted in a series of organic solvents and oxidized using plasma to generate a hydrophillic surface at the channel wall.[28] It has been found that the hydrophilic surface is essential in the synthesis of Cur-PLGA NP as the interaction between nanoparticles and the wall can be significantly reduced to minimize the aggregation inside the microfluidic channel. The uncross-linked low molecular weight oligomers in the PDMS are removed during solvent

extraction and a layer of SiO_2 is generated by air plasma resulting in a stable hydrophilic surface of the channel wall.[28] Milli-Q water was introduced as the continuous phase for all nanoparticle synthesis as shown in Figure 2a. For the synthesis of bare PLGA NP, a stock solution containing $0.5\,\mathrm{mg\,mL^{-1}}$ PLGA in acetone were introduced into the device as dispersed phase. For the synthesis of Cur-PLGA NP, a stock solution containing $0.5\,\mathrm{mg\,mL^{-1}}$ PLGA and $0.05\,\mathrm{mg\,mL^{-1}}$ curcumin (1:10 curcumin:PLGA by weight) in acetone were introduced into the device as dispersed phase (Figure 2a). Both bare PLGA NP and curcumin encapsulated Cur-PLGA NP were successfully synthesized with the fabricated cross slot microfluidic device.

The green fluorescence shown in Figure 2a arises from the emission of curcumin. Curcumin exhibits green fluorescence in organic solvents, however, it is non-fluorescent in water due to efficient fluorescence quenching by water molecules.[32] At low flow rates (i.e., low Reynolds numbers), due to the small dimension of the microchannels, the dispersed phase (curcumin and PLGA in acetone) is squeezed into a narrow focused stream by the two continuous streams (water) as shown in Figure 2a. This significant reduction of the width to approximately 0.6 µm of dispersed phase enables rapid mixing as the diffusion length scale is shortened.[21] A controlled rapid mixing of the dispersed and continuous phase is achieved for the nanoprecipitation due to solvent exchange of the two phases as discussed before.

Effect of flow rate ratio ($R_{\mathbf{flow\ rate}}$)

According to the classical nucleation theory, supersaturation is very important because it determines the nucleation rate, which also depends on the diffusion of curcumin and PLGA molecules.[20] Therefore, rapid mixing of the solvent and the non-solvent phases results in fast nucleation and formation of smaller nuclei.[20] As a result, microfluidics serves as a powerful platform for the nanoprecipitation via solvent exchange because microfluidics enables rapid and controlled mixing of the dispersed and continuous phase.[21,24,25] It has been shown that the width of the focused stream is dependent on the flow rate ratios ($R_{\mathrm{flow\ rate}}$), which is

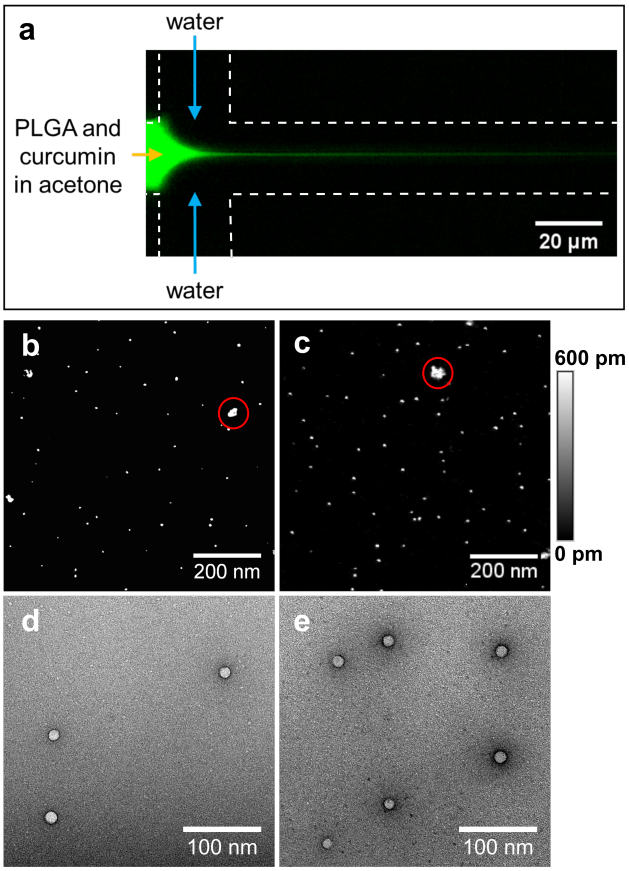

Figure 2: Nanoprecipitation of Cur-PLGA NP by hydrodynamic flow focusing. (a) Fluorescence image of Cur-PLGA NP by nanoprecipitation at the hydrodynamic flow focusing region inside a microfluidic device with 420 nm excitation. The flow rate of water and acetone are 20 µL min^{-1} and 1 µL min^{-1}, respectively. AFM images of the microfluidic synthesized (b) bare PLGA NP and (c) Cur-PLGA NP on mica substrate with a scan area of 800 × 800 nm and the red circles highlight nanoparticle aggregates. TEM images of the (d) bare PLGA NP and (e) Cur-PLGA NP showing spherical shaped nanoparticles.

the flow rate ratio between the dispersed and continuous phases. The smaller the $R_{\text{flow rate}}$, decreases the width of the focused stream, which shortened the diffusion length scale, and hence reduce the time scale for solvent exchange.[21] In order to generate nanoparticle with monodispersity, mixing time must be less than the aggregation time (on the order of ms).[21] The mixing time (τ_{mix}) for solvent exchange can be estimated from $R_{\text{flow rate}}$ using the following relationship[21]

$$\tau_{mix} \approx \frac{w^2}{9D} \frac{1}{(1 + \frac{1}{R_{\text{flow rate}}})^2}, \tag{2}$$

where D is the diffusivity of the solvent and w is the channel width. Equation (2) is an approximation of the timescale for mixing in a 2D hydrodynamic flow focusing configuration, assuming that the velocity of the focused stream is equal to the centerline velocity of the continuous stream.[21] The flow rates of continuous and dispersed phase were controlled using syringe pumps and the flow rate of continuous phase was maintained at $20\,\mu L\,min^{-1}$ while the dispersed phase was varied from 0.5 to $2.5\,\mu L\,min^{-1}$. The predicted mixing times by Equation (2) are in the range of 0.03 to 0.55 ms (Table 1). Further discussion on the effect of $R_{\text{flow rate}}$ on the particle size and size distribution are detailed in the Results Section .

Selection of the PLGA concentrations

It has been reported that polymer concentration in the initial dispersed phase can impact the size of nanoparticles. Diluting the polymer solution leads to a decrease in the particle size and polydispersity.[21,33] This concentration effect has been related to the specific polymer-polymer interactions, which arises when the polymer concentration is above the critical chain overlapping concentration (C^*).[33] A $0.5\,mg\,mL^{-1}$ PLGA in an acetone solution (the concentration used in this study) is well below the C^* of PLGA which is $42.4\,mg\,mL^{-1}$.[34] At this concentration, there is no specific polymer-polymer interactions and the PLGA polymer chains are well solvated by acetone, resulting in independent PLGA chains. Thus, water penetrates in between PLGA chains and promotes small isolated PLGA clusters during nucleation after solvent exchange. Previous study has also shown that the ability to stabilize curcumin with PLGA NP is dependent on the concentration ratio between the curcumin to PLGA used in the synthesis. There is a 3 times reduction in the rate of degradation of curcumin for a 1:10 ratio compared to 1:5 curcumin:PLGA ratio by weight.[6] This enhancement has been attributed to a more efficient encapsulation of curcumin and leads to segregation curcumin from water molecules, which suppresses the hydrolysis of curcumin.[6] Based on these preliminary results, a solution of 1:10 Cur:PLGA in acetone is used to suppress curcumin degradation in all the microfluidic Cur-PLGA NP synthesis in this work.

Selection of the solvent for PLGA

The choice of the solvent is important for the nanoprecipitation of Cur-PLGA NP. Generally, acetone is the most common solvent for the nanoprecipitation of PLGA NP as it is readily miscible with water, easily removed by evaporation and a theta solvent in which PLGA are considered to behave like ideal chains. The interaction between acetone and PLGA is predicted using Bagley's two-dimensional graph shown in the Supporting Information (Figure S.1).[35] A polymer is expected to be soluble in a solvent if the solvent is within the solubility sphere of the polymer and the radius of the solubility sphere is also known as the interaction radius and it is 7.5 for the PLGA used in this study.[36] As shown in Bagley's two-dimensional graph (Supporting Information Figure S.1), acetone is located in the solubility circle of PLGA while water is far away from it, which indicates that acetone is a theta solvent but water is a non-solvent for PLGA.

Characterizations of Cur-PLGA NP

Particle size and size distribution

To confirm the formation of nanoparticles, reaction mixture was collected from the outlet stream of the microfluidic cross slot device and drop-casted on a mica substrate before imaged with atomic force microscopy (AFM). The AFM images of bare PLGA NP and Cur-PLGA NP synthesized with $R_{\text{flow rate}} = 0.05$ are shown in Figure 2b and c. There are some degree of aggregations observed in the dried Cur-PLGA NP sample, which is due to evaporation of the solvent. The identified aggregates (as indicated by the red circles in Figure 2 as an example) are considered as outliers in the size analysis and the diameter of bare PLGA NP and Cur-PLGA NP are 26 ± 3 nm and 24 ± 6 nm, respectively, with a height of less than 600 pm. The flattening of Cur-PLGA NP can be attributed to the dehydration and their strong interaction with the substrate when particles are adsorbed on the mica substrate during the AFM sample preparation. Furthermore, the morphology of the bare PLGA NP

and Cur-PLGA NP are investigated with TEM, see TEM images shown in Figure 2(d,e). The microfluidic synthesized bare PLGA NP and Cur-PLGA NP both exhibit spherical shapes with smooth surfaces.

Table 1: Summary of particle diameter and Zeta potential of the Cur-PLGA NP at various flow rate ratios ($R_{\text{flow rate}}$) resulting in different mixing time (τ_{mix}).

$R_{\text{flow rate}}$	τ_{mix} (ms)	Diameter[a] (nm)	PDI[a,b]	Zeta Potential[a] (mV)	Encapsulation Efficiency[a] (%)
0.025	0.03	32 ± 4	0.13 ± 0.06	-44 ± 1	55 ± 2
0.05	0.10	33 ± 4	0.14 ± 0.02	-58 ± 3	59 ± 5
0.05 [c]	0.10	49 ± 12	0.15 ± 0.02	-44 ± 1	NA
0.05 [d]	0.10	31 ± 2	0.15 ± 0.02	-59 ± 5	NA
0.05 [e]	0.10	29 ± 2	0.15 ± 0.02	-43 ± 3	NA
0.075	0.22	46 ± 7	0.14 ± 0.01	-44 ± 1	67 ± 2
0.1	0.37	52 ± 3	0.11 ± 0.01	-47 ± 3	57 ± 4
0.125	0.55	71 ± 4	0.12 ± 0.01	-58 ± 2	65 ± 3

[a]The reported values are the mean value of three independent experiments and the error values are the standard deviation of the mean.
[b]PDI is derived from the second and third cumulant.[30] The PDI of less than 0.2 indicate monodispersity.
[c]The reported values are for blank PLGA NP.
[d]The reported values are for Cur-PLGA NP after 24 hours.
[e]The reported values are for Cur-PLGA NP after 48 hours.

Next, the hydrodynamic diameters of Cur-PLGA NP synthesized at various flow rates and flow rate ratios $R_{\text{flow rate}}$ were determined from DLS measurements, summarized in Table 1 and the particle size distributions are shown in Figure 3. The rapid mixing by hydrodynamic flow focusing is responsible for the shortened τ_{mix} for solvent exchange.[21] For the $R_{\text{flow rate}}$ used in this study, the estimated τ_{mix} (see Equation (2)) ranges from 0.03 to 0.55 ms. The focused stream becomes narrower when the $R_{\text{flow rate}}$ decreased and mixing is enhanced between the continuous and dispersed phase by significantly reduced τ_{mix}.[21] As a result, a more uniform nucleation is expected and leads to an improved size distribution. Overall,

the Cur-PLGA NP have diameters of less than 100 nm and PDI less than 0.2 for various $R_{\text{flow rate}}$ studied. Furthermore, there is little aggregation observed over a period of 2 days which demonstrates the excellent colloidal stability of these Cur-PLGA NP. The microfluidic synthesized Cur-PLGA NP (30–70 nm in diameter) exhibit smaller particle size than those synthesized using conventional nanoprecipitation (68 ± 16 nm) reported previously.[6] The slight discrepancy in the particle size between the AFM and DLS results is attributable to the fact that the hydrodynamic diameter of Cur-PLGA NP in solution is measured by DLS, which tends to overestimate the particle size.[37]

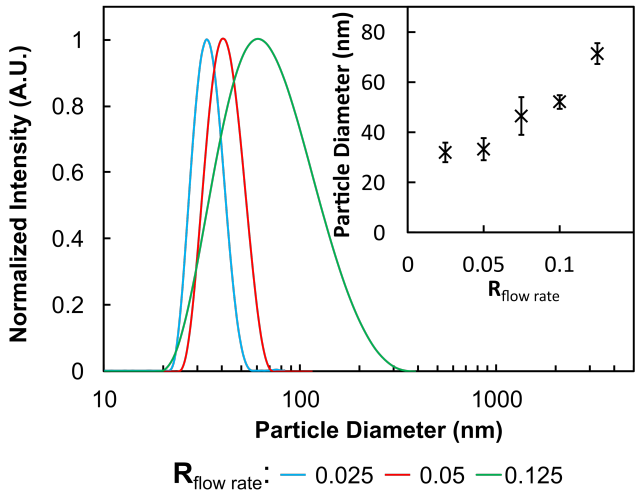

Figure 3: Particle size distribution of Cur-PLGA NP synthesized at various $R_{\text{flow rate}}$. The flow rate of the continuous phase was maintained at 20 µL min^{-1} and the dispersed phase was varied from 0.5 to 2.5 µL min^{-1}. Inset shows the particle size dependence on $R_{\text{flow rate}}$ where results are the mean of three independent experiments and the errors are standard deviation of the mean.

In addition to the effect on particle size, the $R_{\text{flow rate}}$ influences the monodispersity of the synthesized Cur-PLGA NP. Our Cur-PLGA NP are monodispersed as PDI less than 0.2 (Table 1) indicates a homogenous particle population, while a PDI value greater than 0.3 indicates heterogeneity. However, it is important to note that the PDI value from the cummulant method does not distinguish between a broad and a bimodal distribution.[30] Instead of the cummulant method, CONTIN method is used to investigate the particle size distribution as shown in Figure 3.[31] A decrease in the particle size is observed with decreas-

ing $R_{\text{flow rate}}$, the size distribution of Cur-PLGA NP synthesized with a $R_{\text{flow rate}}$ of 0.025 is narrower than those with a $R_{\text{flow rate}}$ of 0.125 (Figure 3). For the formation of NP with low PDI, rapid mixing is essential for homogeneous supersaturation of solution, which is achieved with a short mixing time (as summarized in Table 1) to ensure uniform nucleation.[20,21] A decrease in the particle diameter is accompanied by improved size distribution with decreasing $R_{\text{flow rate}}$ (Figure 3), which is in good agreement with a previous study on microfluidic assisted synthesis of polymer NP.[21] Furthermore, the size distribution dependency on $R_{\text{flow rate}}$ suggests that the rate of particle growth is slower than the τ_{mix}.[21] Since our Cur-PLGA NP synthesized using nanoprecipitation principle in a microfluidic device yield monodispersed particles with particle diameters less than 100 nm, Cur-PLGA NP are expected to improve the bioavailability of curcumin and the subsequent accumulation in tumors due to the EPR effect.

Colloidal stability

To examine the colloidal stability of the Cur-PLGA NP, its zeta potentials are measured by an electrophoretic light scattering spectrophotometer (ELZS-2000). The Cur-PLGA NP exhibit negative zeta potentials ranging from -44 to -58 mV (Table 1) and it is in good agreement with previous studies of Cur-PLGA NP synthesized by conventional nanoprecipitation method.[1,6] The negatively charged surface of the Cur-PLGA NP indicates excellent colloidal stability, as the electrostatic repulsive interaction is greater than the attractive van der Waals interaction among Cur-PLGA NP, resulting a stable aqueous suspension. Note that there is no observable aggregation within the time of measurement (Supporting Information Figure S.3).

Stability of the PLGA NP encapsulated curcumin

Next, we investigate the stability of Cur-PLGA NP with UV-visible absorption spectroscopy (Shimadzu UV-1800). Figure 4 shows the UV-visible spectra of Cur-PLGA NP over time.

We observe a strong absorption in the UV-visible spectral region with absorption maximum at 422 nm and two shoulders around 350 and 450 nm, as shown in Figure 4 (arrows). The absorption band observed at 422 nm is attributed to the $\pi-\pi^*$ transition of curcumin as PLGA are optically transparent in the visible spectrum.[6,38] In addition to the absorption peaks, a shoulder in the absorption spectrum is also observed at 450 nm which is absent in the absorption spectrum curcumin in an aqueous environment[16] (Figure 4). The UV-visible absorption spectrum of curcumin in PLGA NP agrees well with curcumin in dimethylformamide (DMF), which indicates that curcumin is likely to be located in an environment that is similar to DMF.[32] Therefore, the enhanced stability of curcumin encapsulated inside PLGA NP compared to native curcumin is due to its segregation from the aqueous environment. As water molecules are absent in the hydrophobic regions of the PLGA NP, the suppression of hydrolysis of curcumin, which is the major pathway of degradation of curcumin, can be achieved using PLGA NP.

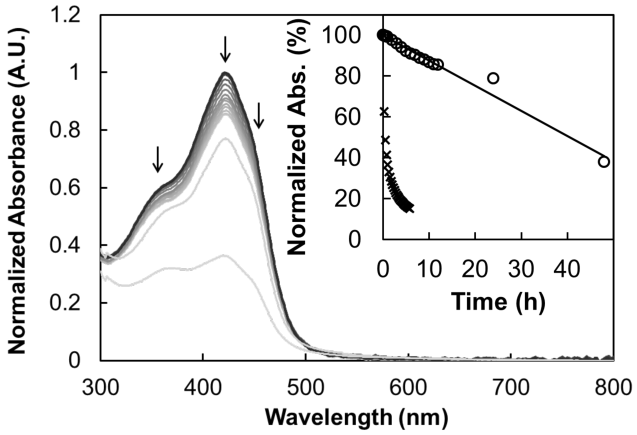

Figure 4: Kinetic UV-visible absorption spectra of Cur-PLGA NP ($R_{\text{flow rate}}$=0.05) at 37 °C with inset showing the decrease of absorbance at 422 nm over time of Cur-PLGA NP (circles), fitted with the pseudo-zero-order kinetic model (solid line), and native curcumin in water (crosses).

As the absorption maximum at 422 nm is due to the presence of curcumin in PLGA NP, the stability of native curcumin in water and curcumin encapsulated in PLGA NP was determined by monitoring the change in absorbance at this wavelength over time (Figure 4 inset). The striking difference between the degradation of native curcumin and Cur-

PLGA NP demonstrated the excellent stabilization of curcumin encapsulated by PLGA NP. The decrease in absorbance signifies a depletion of curcumin which is attributed to the degradation of curcumin and the slow decay of Cur-PLGA NP is fitted to a pseudo-zero-order kinetic model (represented as a solid line in the inset of Figure 4). The pseudo-zero-order kinetics has been observed in the curcumin degradation,[39] while the rate of curcumin degradation is $1.1 \pm 0.4\,\%\,\mathrm{h}^{-1}$ when encapsulated in our microfluidic synthesized PLGA NP. The PLGA NP encapsulated curcumin has an extended half life of approximately 2 days compared to $\sim$30 min for the native curcumin in water (Figure 4 inset) as expected.[15,16] It has been proposed that curcumin is encapsulated in the hydrophobic regions of PLGA NP, which results in curcumin segregated from water and suppresses hydrolysis of curcumin.[6]

The encapsulation efficiency is calculated according to Equation 1 and the values are summarized in Table 1. Overall, the encapsulation efficiency of our Cur-PLGA NP is around 55 to 67 %. Our Cur-PLGA NP has a moderate encapsulation efficiency of curcumin compared to other curcumin nanoparticle systems with an encapsulation efficiency ranges from 50 to 90 %.[10,40,41] It has been shown that the encapsulation efficiency is dependent on the present stabilizer as the addition of stabilizer enhances the swelling of PLGA NP to encapsulate curcumin.[41] Analysis on the Hansen solubility parameters of curcumin and PLGA have shown that curcumin is able to be encapsulated within the PLGA NP by forming a homogeneous mixture with the PLGA NP.[6] As a result, curcumin is expected to be uniformly distributed inside PLGA NP resulting in segregation from the aqueous environment and exhibits stability inside PLGA NP. Similar to a previous study,[6] the volume of Cur-PLGA NP ($R_{\text{flow rate}} = 0.05$) was calculated based on the average diameter of 33 nm (Table 1) and the average number of curcumin per nanoparticle was estimated to be 7.6×10^3. Our microfluidic synthesized PLGA NP exhibit effective encapsulation and stabilization of curcumin, therefore, it is expected that Cur-PLGA NP has the potential as delivery system for curcumin and improves the bioavailability of curcumin.

Cellular uptake of curcumin

We show proof of concept studies of using the microfluidic synthesized Cur-PLGA NP as nontoxic and effective delivery system for curcumin without perturbing its medicinal properties. First, we assessed the ability of the synthesized Cur-PLGA NP delivering curcumin to leukemia Jurkat and NIH3T3 fibroblast cell lines. The amount of cellular uptake were monitored using confocal fluorescence microscopy. Figure 5 shows the fluorescence images of leukemia Jurkat cells incubated with 6 µM native curcumin and Cur-PLGA NP containing 6 µM of curcumin for 4 hours and 2 days. An aliquot of 1 mg mL^{-1} curcumin in acetone stock solution was used to yield 6 µM of curcumin. The blue fluorescence is due to the nucleus Hoechst stain with 350 nm excitation and the fluorescence intensity is constant across the media control and various treatments. The microfluidic synthesized Cur-PLGA NP exhibit green fluorescence emission (maximum at 500 nm) upon excitation with 420 nm (Supporting Information Figure S.4). This green fluorescence emission is in excellent agreement with previous studies and it is attributed to the emission of curcumin encapsulated in PLGA NP.[6,32] Therefore, the green fluorescence observed with confocal microscopy is attributed to the combination of intrinsic cell fluorescence and curcumin fluorescence for cells with curcumin treatments. Cellular uptake of Cur-PLGA NP by NIH3T3 fibroblast cells were also monitored and similar observations were made (Supporting Information Figure S.5).

The mean green fluorescence intensity was determined and compared for various treatments with leukemia Jurkat and NIH3T3 fibroblast cells as shown in Figure 6. We observed no specificity in the curcumin delivery as the fluorescence intensity increased in both leukemia Jurkat and NIH3T3 fibroblast cell lines treated with Cur-PLGA NP compared to the media control (without curcumin treatment). The fluorescence increases after 4 hours of incubation (Figure 6, blue bars) in both leukemia Jurkat and NIH3T3 cell lines. This significant increase in the fluorescence intensity inside leukemia Jurkat and NIH3T3 fibroblast cell lines with Cur-PLGA NP or native curcumin compared to the media control implies that there is a higher cellular concentration of curcumin. The overall fluorescence intensity in leukemia

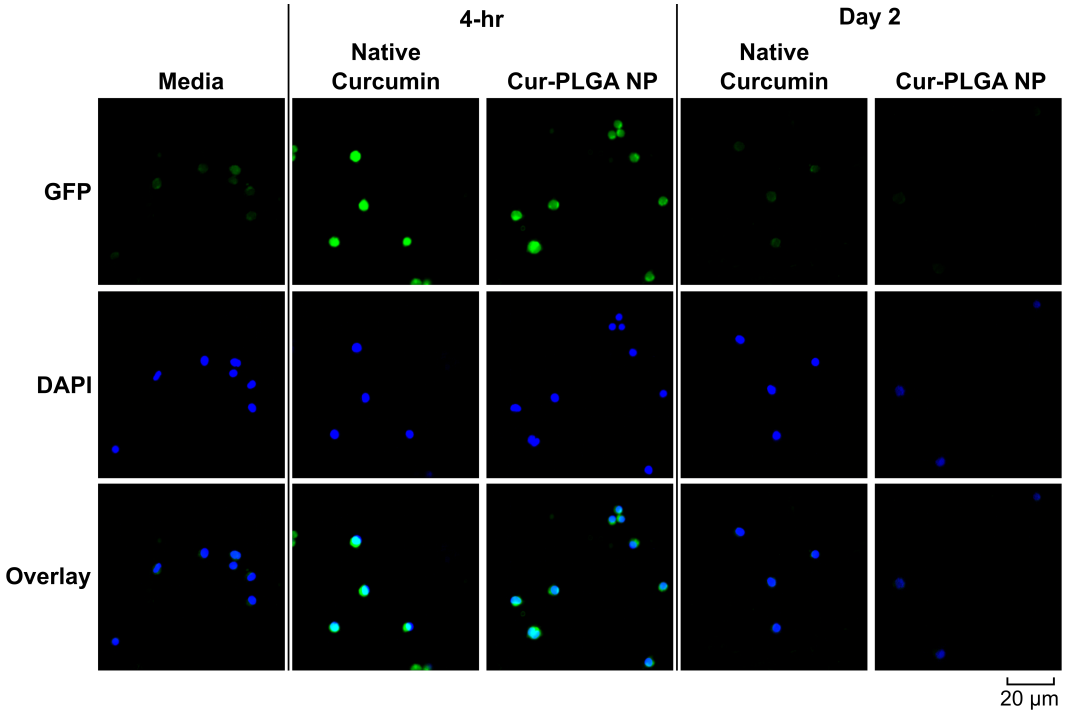

Figure 5: Confocal fluorescence image of Jurkat cells in the media control, treated with 6 µM of native curcumin and with the equivalent curcumin concentration of Cur-PLGA NP for 4 h and 2 days. Images were taken with 20x magnification. Rows from top to bottom: curcumin fluorescence (excitation at 420 nm), cell nuclei stained with Hoechst (excitation at 350 nm) and overlaid image of curcumin and Hoechst fluorescence.

Jurkat cell is similar to the NIH3T3 fibroblast cell with the same treatments of native curcumin or Cur-PLGA-NP. As the cellular autofluorescence of NIH3T3 fibroblast is higher than leukemia Jurkat cell, the fluorescence intensity increase is greater in leukemia Jurkat cell than NIH3T3 fibroblast. This increase in the fluorescence intensity (blue bars, Figure 6) has been ascribed to the hydrophobic environments of tumor cells.[42] These results have demonstrated that the PLGA NP do not alter the cell uptake of curcumin by both leukemia Jurkat and NIH3T3 fibroblast cells.

The overall fluorescence intensity of cells with Cur-PLGA NP and native curcumin treatments decreases after 2 days (Figure 6, red bars) indicating that there are less curcumin present in cells. Furthermore, the decrease in fluorescence intensity for both cell lines with Cur-PLGA NP treatment is less than those treated with native curcumin. The higher fluorescence intensity indicates there are more curcumin present in cells and this can be attributed

to the stabilization of curcumin by PLGA NP (Figure 4). Interestingly, there are more curcumin uptake in Jurkat cell with 4 hours of native curcumin incubation than Cur-PLGA NP (Figure 6 (left, blue bars)), however, there are less native curcumin than Cur-PLGA NP after 2 days of incubation (Figure 6 (left, red bars)). Overall, Cur-PLGA NP is a better delivery system for curcumin as the amount of cellular curcumin deliver by Cur-PLGA NP is higher than native curcumin in both Jurkat and NIH3T3 fibroblast cell lines (Figure 6, red bars).

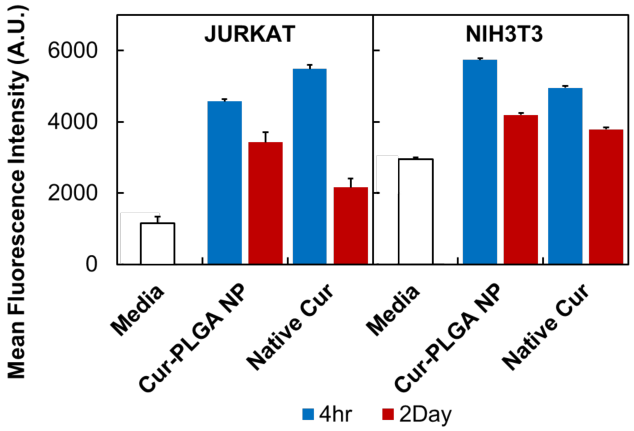

Figure 6: Cellular uptake of curcumin and Cur-PLGA NP by leukemia Jurkat (right) and NIH3T3 fibroblast (left) cells after 4 h (blue bars) and 2 days (red bars) of incubation in triplicates. The results shown are the median fluorescence intensity and the errors are coefficient of variation of the median.

Cell viability with curcumin treatment

We next investigate the cell viability of leukemia Jurkat and NIH3T3 fibroblast cell lines with Cur-PLGA NP treatment. The effect of Cur-PLGA NP on the viability of leukemia Bcl-2 (S70A) Jurkat and NIH3T3 fibroblast cells were evaluated and the results are shown in Figure 7. In comparison with all control treatments, cell viability decreased in Jurkat cell with both native curcumin and the Cur-PLGA NP treatment. Cell viability have dropped to 74 % and 56 % for native curcumin and the Cur-PLGA NP treatments (yellow and white bars respectively in Figure 7), despite of its resistance to apoptosis via phosphorylation of

Bcl-2 proteins at serine 70.[43] It has been reported that the curcumin-induced Jurkat cells apoptosis is independent of the level of Bcl-2 protein.[44] Additionally, Jurkat cells apoptosis is linked to the elevated level of cellular glutathione induced by curcumin.[45]

Since the cell uptake results confirmed that there are same cellular concentration of curcumin in Jurkat by native curcumin and the Cur-PLGA NP treatments (Figure 6), the difference in the cell viability of Jurkat cells is obviously not caused by the cellular concentration of curcumin alone, but also related to the stability of curcumin. Although similar cell uptake trend of curcumin is observed in NIH3T3 fibroblast cells, there is no decrease on the cell viability for all the treatments (Figure 7), verifying that native curcumin and the Cur-PLGA NP are nontoxic to NIH3T3 fibroblast cells, consistent with previous reports at comparable curcumin dosages.[3,46] For example, it has been reported that there is no observable effect on NIH3T3 cells viability up to 20 µM dosage of curcumin, while another study has shown there is no effect on the growth of NIH3T3 cell up to 1 mM of curcumin.[46]

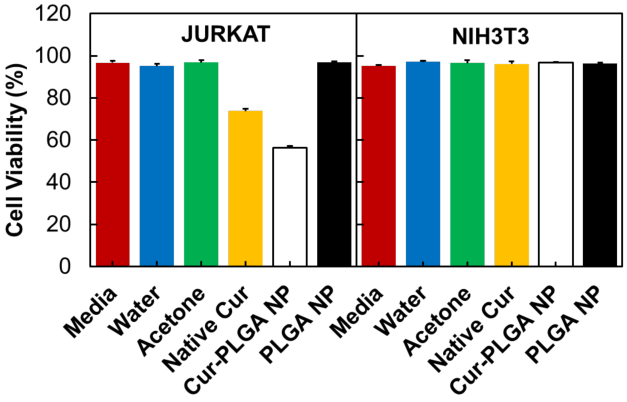

Figure 7: Cell viability assays on Jurkat (left) and NIH3T3 fibroblast (right) cells treated with 5 µM of curcumin; and with the equivalent curcumin concentration of Cur-PLGA NP, along with cell culture media, water, acetone and blank PLGA NP control experiments for 2 days. The results shown are the mean of triplicates and the errors are standard deviation of the mean.

To evaluate the effect of Cur-PLGA NP against Jurkat cell, we also conducted dosage dependent cytotoxicity of Cur-PLGA NP. Jurkat cells exhibit a dosage response with the concentration of curcumin in Cur-PLGA NP over a period of 2 day incubation after a single dosage. An increase in the cell death is observed with increasing curcumin concentration in

the Cur-PLGA NP solution as shown in Figure 8. The 50 % maximal inhibitory response (IC_{50}) is about 5.3 µM, which is calculated from the sigmoidal fit (Figure 8, solid curve). Our results are comparable to other studies, which have shown that the IC_{50} of curcumin is between 3 to 14 µM for Jurkat cells.[47,48]

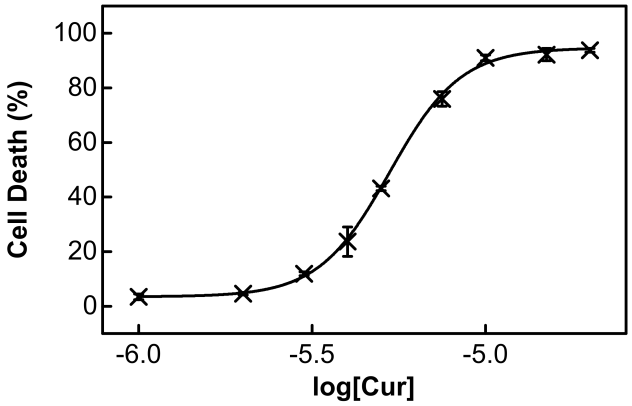

Figure 8: Dosage response of Jurkat cells to Cur-PLGA NP between 1 to 10 µM of curcumin over a period of 2 days after a single dosage. Results are presented as the mean of three independent experiments and the reported error is the standard deviation of the mean. The IC_{50} is about 5.3 µM calculated from a sigmoidal fitting (solid curve). Note that x-axis is the log of curcumin concentration in the Cur-PLGA NP determined by UV-visible spectroscopy.

CONCLUSIONS

The ability to control particle size of nanoparticles is critical for its biodistribution and cellular uptake. A size tunable synthesis of Cur-PLGA NP using a microfluidic hydrodynamic flow focusing platform has been demonstrated. The resulting Cur-PLGA NP are less than 100 nm in diameter with a narrow size distribution and excellent colloidal stability. Our Cur-PLGA NP significantly inhibit the degradation of curcumin with the rate of degradation of $1.1 \pm 0.4\,\% \,\mathrm{h}^{-1}$. Our microfluidic synthesized Cur-PLGA NP is a nontoxic and effective delivery system for curcumin, in particular, it enhances anti-cancer activity of curcumin against leukemia Jurkat cells compared to native curcumin. Our findings motivate the application of microfluidic technologies for the synthesis of polymer nanoparticle for effective drug delivery.

Acknowledgement

We gratefully acknowledge support from the Okinawa Institute of Science and Technology Graduate University (OIST) with subsidy funding from the Cabinet Office, Government of Japan. A.Q.S and M.L. also acknowledge funding from the Japanese Society for the Promotion of Science (Grants-in-Aid for Scientific Research (C) grant number JP17K06173, and Grant-in-Aid for JSPS Research Fellow grant number JP16F16720, respectively). We thank Mr. Kazumi Toda-Peters and Mr. Kei Funakoshi from Micro/Bio/nanofluidics Unit at OIST for their help with the microfabrication work, Dr. Riccardo Funari from Micro/Bio/nanofluidics Unit at OIST for his help in the AFM experiments, Mr. Toshio Sasaki from the Imaging Section, Research Support Division at OIST for his help in TEM experiments and Mr. Hsieh-Fu Tsai and Miss Shivani Sathish from Micro/Bio/nanofluidics Unit at OIST for their help with the cell culture.

Supporting Information Available

The following files are available free of charge.

- Bagley's two-dimensional graph of the partial solubility parameters of acetone, water and PLGA.
- Standard curve for the determination of the amount of curcumin in Cur-PLGA NP
- Consecutive measurements on the particle size distribution and zeta potential of Cur-PLGA NP.
- UV-vis absorption and fluorescence emission spectra of Cur-PLGA NP.
- Confocal fluorescence image of NIH3T3 fibroblast cells in media control, treated with 6 µM of curcumin and with the the equivalent curcumin concentration of Cur-PLGA NP for 4 hours and 2 days.

This material is available free of charge via the Internet at `http://pubs.acs.org/`.

References

(1) Punfa, W.; Yodkeeree, S.; Pitchakarn, P.; Ampasavate, C.; Limtrakul, P. Enhancement of Cellular Uptake and Cytotoxicity of Curcumin-Loaded PLGA Nanoparticles by Conjugation with Anti-p-Glycoprotein in Drug Resistance Cancer Cells. *Acta Pharmacol. Sin.* **2012**, *33*, 823–831.

(2) Zaman, M. S.; Chauhan, N.; Yallapu, M. M.; Gara, R. K.; Maher, D. M.; Kumari, S.; Sikander, M.; Khan, S.; Zafar, N.; Jaggi, M.; Chauhan, S. C. Curcumin Nanoformulation for Cervical Cancer Treatment. *Sci. Rep.* **2016**, *6*, 20051.

(3) Chopra, D.; Ray, L.; Dwivedi, A.; Tiwari, S. K.; Singh, J.; Singh, K. P.; Kushwaha, H. N.; Jahan, S.; Pandey, A.; Gupta, S. K.; Chaturvedi, R. K.; Pant, A. B.; Ray, R. S.; Gupta, K. C. Photoprotective Efficiency of PLGA-Curcumin Nanoparticles Versus Curcumin Through the Involvement of ERK/AKT Pathway under Ambient UV-R Exposure in HaCaT Cell Line. *Biomaterials* **2016**, *84*, 25–41.

(4) Chernenko, T.; Matthäus, C.; Milane, L.; Quintero, L.; Amiji, M.; Diem, M. Label-Free Raman Spectral Imaging of Intracellular Delivery and Degradation of Polymeric Nanoparticle Systems. *ACS NANO* **2009**, *3*, 3552–3559.

(5) Tracy, M.; Ward, K.; Firouzabadian, L.; Wang, Y.; Dong, N.; Qian, R.; Zhang, Y. Factors Affecting the Degradation Rate of Poly(lactide-co-glycolide) Microspheres *in vivo* and *in vitro*. *Biomaterials* **1999**, *20*, 1057–1062.

(6) Leung, M. H. M.; Harada, T.; Dai, S.; Kee, T. W. Nanoprecipitation and Spectroscopic Characterization of Curcumin-Encapsulated Polyester Nanoparticles. *Langmuir* **2015**, *31*, 11419–11427.

(7) Duo, X.; Li, Q.; Wang, J.; Lv, J.; Hao, X.; Feng, Y.; Ren, X.; Shi, C.; Zhang, W. Core/Shell Gene Carriers with Different Lengths of PLGA Chains to Transfect Endothelial Cells. *Langmuir* **2017**, *33*, 13315–13325.

(8) Garbuzenko, O. B.; Winkler, J.; Tomassone, M. S.; Minko, T. Biodegradable Janus Nanoparticles for Local Pulmonary Delivery of Hydrophilic and Hydrophobic Molecules to the Lungs. *Langmuir* **2014**, *30*, 12941–12949.

(9) Yang, F. S.; Lim, G. P.; Begum, A. N.; Ubeda, O. J.; Simmons, M. R.; Ambegaokar, S. S.; Chen, P. P.; Kayed, R.; Glabe, C. G.; Frautschy, S. A.; Cole, G. M. Curcumin Inhibits Formation of Amyloid β Oligomers and Fibrils, Binds Plaques, and Reduces Amyloid *in Vivo*. *J. Biol. Chem.* **2005**, *280*, 5892–5901.

(10) Chereddy, K. K.; Coco, R.; Memvanga, P. B.; Ucakar, B.; des Rieux, A.; Vandermeulen, G.; Preat, V. Combined Effect of PLGA and Curcumin on Wound Healing Activity. *J. Controlled Release* **2013**, *171*, 208–215.

(11) Cartiera, M. S.; Ferreira, E. C.; Caputo, C.; Egan, M. E.; Caplan, M. J.; Saltzman, W. M. Partial Correction of Cystic Fibrosis Defects with PLGA Nanoparticles Encapsulating Curcumin. *Mol. Pharm.* **2010**, *7*, 86–93.

(12) Zhao, J.; Liu, J.; Xu, S.; Zhou, J.; Han, S.; Deng, L.; Zhang, J.; Liu, J.; Meng, A.; Dong, A. Graft Copolymer Nanoparticles with pH and Reduction Dual-Induced Disassemblable Property for Enhanced Intracellular Curcumin Release. *ACS Appl. Mater. Interfaces* **2013**, *5*, 13216–13226.

(13) Kaminaga, Y.; Nagatsu, A.; Akiyama, T.; Sugimoto, N.; Yamazaki, T.; Maitani, T.; Mizukami, H. Production of Unnatural Glucosides of Curcumin with Drastically Enhanced Water Solubility by Cell Suspension Cultures of Catharanthus Roseus. *FEBS Lett.* **2003**, *555*, 311–316.

(14) Letchford, K.; Liggins, R.; Burt, H. Solubilization of Hydrophobic Hrugs by Methoxy Poly(ethylene glycol)-block-polycaprolactone Diblock Copolymer Micelles: Theoretical and Experimental Data and Correlations. *J. Pharm. Sci.* **2008**, *97*, 1179–1190.

(15) Wang, Y. J.; Pan, M. H.; Cheng, A. L.; Lin, L. I.; Ho, Y. S.; Hsieh, C. Y.; Lin, J. K. Stability of Curcumin in Buffer Solutions and Characterization of its Degradation Products. *J. Pharm. Biomed. Anal.* **1997**, *15*, 1867–1876.

(16) Harada, T.; Pham, D.-T.; Leung, M. H. M.; Ngo, H. T.; Lincoln, S. F.; Easton, C. J.; Kee, T. W. Cooperative Binding and Stabilization of the Medicinal Pigment Curcumin by Diamide linked γ-Cyclodextrin Dimers: A Spectroscopic Caracterization. *J. Phys. Chem. B* **2011**, *115*, 1268–1274.

(17) Sa, G.; Das, T. Anti-Cancer Effects of Curcumin: Cycle of Life and Death. *Cell Division* **2008**, *3*, 1–14.

(18) Fillafer, C.; Wirth, M.; Gabor, F. Stabilizer-Induced Viscosity Alteration Biases Nanoparticle Sizing via Dynamic Light Scattering. *Langmuir* **2007**, *23*, 8699–8702.

(19) Bertrand, N.; Grenier, P.; Mahmoudi, M.; Lima, E. M.; Appel, E. A.; Dormont, F.; Lim, J.-M.; Karnik, R.; Langer, R.; Farokhzad, O. C. Mechanistic Understanding of *in vivo* Protein Corona Formation on Polymeric Nanoparticles and Impact on Pharmacokinetics. *Nat. Commun.* **2017**, *8*, 777.

(20) Lepeltier, E.; Bourgaux, C.; Couvreur, P. Nanoprecipitation and the "Ouzo Effect": Application to Drug Delivery Devices. *Adv. Drug Delivery Rev.* **2014**, *71*, 86–97.

(21) Karnik, R.; Gu, F.; Basto, P.; Cannizzaro, C.; Dean, L.; Kyei-Manu, W.; Langer, R.; Farokhzad, O. C. Microfluidic Platform for Controlled Synthesis of Polymeric Nanoparticles. *Nano Lett.* **2008**, *8*, 2906–2912.

(22) Maeda, H. Macromolecular Therapeutics in Cancer Treatment: the EPR Effect and Beyond. *J. Controlled Release* **2012**, *164*, 138–144.

(23) Dufort, S.; Sancey, L.; Coll, J.-L. Physico-Chemical Parameters that Govern Nanoparticles Fate also Dictate Rules for Their Molecular Evolution. *Adv. Drug Delivery Rev.* **2012**, *64*, 179–189.

(24) Ma, J.; Lee, S. M.-Y.; Yi, C.; Li, C.-W. Controllable Synthesis of Functional Nanoparticles by Microfluidic Platforms for Biomedical Applications–A Review. *Lab. Chip* **2017**, *17*, 209–226.

(25) Xu, J.; Zhang, S.; Machado, A.; Lecommandoux, S.; Sandre, O.; Gu, F.; Colin, A. Controllable Microfluidic Production of Drug-Loaded PLGA Nanoparticles Using Partially Water-Miscible Mixed Solvent Microdroplets as a Precursor. *Sci. Rep.* **2017**, *7*, 4794.

(26) Lazarus, L. L.; Riche, C. T.; Marin, B. C.; Gupta, M.; Malmstadt, N.; Brutchey, R. L. Two-Phase Microfluidic Droplet Flows of Ionic Liquids for the Synthesis of Gold and Silver Nanoparticles. *ACS Appl. Mater. Interfaces* **2012**, *4*, 3077–3083.

(27) Friend, J.; Yeo, L. Fabrication of Microfluidic Devices Using Polydimethylsiloxane. *Biomicrofluidics* **2010**, *4*, 026502.

(28) Vickers, J. A.; Caulum, M. M.; Henry, C. S. Generation of Hydrophilic Poly(dimethylsiloxane) for High-Performance Microchip Electrophoresis. *Anal. Chem.* **2006**, *78*, 7446–7452.

(29) Schneider, C. A.; Rasband, W. S.; Eliceiri, K. W. NIH Image to ImageJ: 25 Years of Image Analysis. *Nat. Methods* **2012**, *9*, 671–675.

(30) Frisken, B. J. Revisiting the Method of Cumulants for the Analysis of Dynamic Light-Scattering Data. *Appl. Opt.* **2001**, *40*, 4087–4091.

(31) Provencher, S. W. CONTIN: A General Purpose Constrained Regularization Program for Inverting Noisy Linear Algebraic and Integral Equations. *Comput. Phys. Commun.* **1982**, *27*, 229–242.

(32) Chignell, C. F.; Bilskj, P.; Reszka, K. J.; Motten, A. G.; Sik, R. H.; Dahl, T. A. Spectral and Photochemical Properties of Curcumin. *Photochem. Photobiol.* **1994**, *59*, 295–302.

(33) Legrand, P.; Lesieur, S.; Bochot, A.; Gref, R.; Raatjes, W.; Barratt, G.; Vauthier, C. Influence of Polymer Behaviour in Organic Solution on the Production of Polylactide Nanoparticles by Nanoprecipitation. *Int. J. Pharm.* **2007**, *344*, 33–43.

(34) Wan, F.; Baldursdottir, S. G.; Maltesen, M. J.; Bjerregaard, S.; Foged, C.; Rantanen, J.; Yang, M. PLGA Conformational Behaviour Dependence of the Network Characterized by Rheological Study. *Nordic Rheology Society. Annual Transactions* **2013**, *21*, 357–361.

(35) Bagley, E.; Nelson, T.; Scigliano, J. Three-Dimensional Solubility Parameters and Their Relationship to Internal Pressure Measurements in Polar and Hydrogen Bonding Solvents. *J. Paint Technol.* **1971**, *43*, 35–42.

(36) Schenderlein, S.; Lück, M.; Müller, B. Partial Solubility Parameters of Poly(d,l-lactide-co-glycolide). *Int. J. Pharm.* **2004**, *286*, 19–26.

(37) Kumar, M. R.; Bakowsky, U.; Lehr, C. Preparation and Characterization of Cationic PLGA Nanospheres as DNA Carriers. *Biomaterials* **2004**, *25*, 1771–1777.

(38) Wang, Z. F.; Leung, M. H. M.; Kee, T. W.; English, D. S. The Role of Charge in the Surfactant-Assisted Stabilization of the Natural Product Curcumin. *Langmuir* **2010**, *26*, 5520–5526.

(39) Bernabé-Pineda, M.; Ramírez-Silva, M. T.; Romero-Romo, M.; González-Vergara, E.; Rojas-Hernández, A. Determination of Acidity Constants of Curcumin in Aqueous So-

lution and Apparent Rate Constant of its Decomposition. *Spectrochim. Acta, Part A* **2004**, *60*, 1091–1097.

(40) Khalil, N. M.; do Nascimento, T. C. F.; Casa, D. M.; Dalmolin, L. F.; de Mattos, A. C.; Hoss, I.; Romano, M. A.; Mainardes, R. M. Pharmacokinetics of Curcumin-Loaded PLGA and PLGA-PEG Blend Nanoparticles after Oral Administration in Rats. *Colloids Surf. B* **2013**, *101*, 353–360.

(41) Yallapu, M. M.; Gupta, B. K.; Jaggi, M.; Chauhan, S. C. Fabrication of Curcumin Encapsulated PLGA Nanoparticles for Improved Therapeutic Effects in Metastatic Cancer Cells. *J. Colloid Interface Sci.* **2010**, *351*, 19–29.

(42) Kunwar, A.; Barik, A.; Mishra, B.; Rathinasamy, K.; Pandey, R.; Priyadarsini, K. Quantitative Cellular Uptake, Localization and Cytotoxicity of Curcumin in Normal and Tumor Cells. *Biochim. Biophys. Acta, Gen. Subj.* **2008**, *1780*, 673–679.

(43) Yamamoto, K.; Ichijo, H.; Korsmeyer, S. J. BCL-2 Is Phosphorylated and Inactivated by an ASK1/Jun N-Terminal Protein Kinase Pathway Normally Activated at G2/M. *Mol. Cell. Biol.* **1999**, *19*, 8469–8478.

(44) Piwocka, K.; Zabłocki, K.; Więkowski, M. R.; Skierski, J.; Feiga, I.; Szopa, J.; Drela, N.; Wojtczak, L.; Sikora, E. A Novel Apoptosis-like Pathway, Independent of Mitochondria and Caspases, Induced by Curcumin in Human Lymphoblastoid T (Jurkat) Cells. *Exp. Cell. Res.* **1999**, *249*, 299–307.

(45) Sandur, S. K.; Pandey, M. K.; Sung, B.; Ahn, K. S.; Murakami, A.; Sethi, G.; Limtrakul, P.; Badmaev, V.; Aggarwal, B. B. Curcumin, Demethoxycurcumin, Bisdemethoxycurcumin, Tetrahydrocurcumin and Turmerones Differentially Regulate Anti-Inflammatory and Anti-Proliferative Responses Through a ROS-Independent Mechanism. *Carcinogenesis* **2007**, *28*, 1765–1773.

(46) Karewicz, A.; Bielska, D.; Loboda, A.; Gzyl-Malcher, B.; Bednar, J.; Jozkowicz, A.; Dulak, J.; Nowakowska, M. Curcumin-Containing Liposomes Stabilized by Thin Layers of Chitosan Derivatives. *Colloids Surf., B* **2013**, *109*, 307–316.

(47) Gertsch, J.; Güttinger, M.; Heilmann, J.; Sticher, O. Curcumin Differentially Modulates mRNA Profiles in Jurkat T and Human Peripheral Blood Mononuclear Cells. *Bioorg. Med. Chem.* **2003**, *11*, 1057–1063.

(48) Gopal, P. K.; Paul, M.; Paul, S. Curcumin Induces Caspase Mediated Apoptosis in JURKAT Cells by Disrupting the Redox Balance. *Asian Pac. J. Cancer Prev.* **2014**, *15*, 93–100.

Graphical TOC Entry